

Simulation Study of a Novel Subgrid Model for Microtopography Effect on Surface Flow

Abstract

A subgrid model for accurate representation of surface flow behavior, influenced by surface microtopography, at larger spatial scales is presented. It is well understood that the spatial heterogeneity in the surface microtopography serves a critical role in the surface water retention, surface/subsurface interactions, and delay runoff, and thereby significantly affects the shape of the hydrographs. But high-resolution simulations at large spatial and temporal scales are not tractable. Watershed-scale simulations demand to alter the accumulation term and the flow law in the governing equation of the surface flow to incorporate the effect of surface microtopography on the water storage and the discharge rate, and hence motivates the idea of subgrid representation. Simulations have been carried out and numerical results of the subgrid model are compared to that of without subgrid model and fine-scale results of seven ice-wedge polygons. A good match between the fine-scale simulations and the subgrid model results confirms that our subgrid model improved the shape of the hydrographs and the total water content in the system. Furthermore, the model is applied to a 468 polygons catchment, and significant changes are observed in the results of with and without subgrid model. The results of the developed model highlight that the model is able to achieve fine-scale behavior at larger spatial scales.

Keywords: Subgrid model, Permafrost, Microtopography, Hydrograph,

1. Introduction

To gain insight into the role of heterogeneous spatial structure of the ground surface is important for understanding interactions between surface and subsurface, surface runoff and discharge rate. Numerical models must
 5 be able to incorporate fine-scale spatial variability through a subgrid model representation when conducting simulations with low resolution grids – an extended version of the existing models is required to account for fine-scale surface flow behavior.

When rainfall dominates the infiltration, surface runoff happens. The
 10 surface runoff and the shape of the hydrographs could significantly be affected by the spatially varying surface microtopography (unevenness at small scale). The importance of the microtopography cannot be ignored for accurate representation of the surface processes. From simulations perspective, an accurate flow behavior is captured at the fine-scale (a scale of centime-
 15 ters), however, fine-scale simulations are computationally expensive. In addition, most of the field observations are made at the fine-scale, and the lack of high spatial resolution data at the watershed scale, surface microtopographic effects on the runoff are usually ignored at larger spatial scales. A subgrid model is build on the information gained from highly resolved
 20 surface topographic data; the depressions and obstructions. Depressions are disconnected low points in the topography (surface pits) and retains water that is available only for infiltration or/and evaporation. On the other hand, obstructions exits above the depressions and interrupt and slow the flow, but do not completely block it. To capture these effects in a model,
 25 the depressions require to change the accumulation term and obstructions

need to introduce a friction factor to influence the surface flow term and hence surface detention.

The integrated surface/subsurface modeling has received considerable attention from researchers across the world; see, for example, [1, 2, 3] and
30 references therein. Here we focus only on the subgrid modeling approach. Though the concept of microtopographic features and their implications on the flow and discharge is not new, but has not been fully addressed and understood from modeling perspective. Accurate representation of surface microtopography in a coupled surface/subsurface hydrologic model at
35 watershed-scale is a challenging task. In the mid-1950s, the significance of the surface microtopographic features were described in [4]. Panday and Huyakorn (2004) presented an integrated surface/subsurface flow model with subgrid representation through the surface depressions and obstructions by modifying the overland flow governing equation. **INCOMPLETE!!**

40 The rest of the paper is organized as follows. Section 2 introduces the derivation of the governing equations of the subgrid model. A short description, for a quick reference, of the Advanced Terrestrial Simulator (ATS) and the Arcos multiphysics management framework, within which we implemented our subgrid model, is presented in Section 3. In Section 4 we
45 compare the numerical results of our subgrid model with no subgrid model and fine-scale results to illustrate the accuracy of our subgrid model for capturing fine-scale microtopographic features. Finally, in Section 5, we offer closing remarks and future research inline with thaw-induced subsidence.

2. Subgrid Model

This section describes the derivation of the subgrid model. The subgrid model alters the accumulation term and the flow law. For example, the ponded depth in the accumulation term is typically replaced with a volumetric depth, the ponded depth that would occur if the surface were flat. Specifically, we make the substitution in the accumulation term, where is ponded depth. The volumetric head may be calculated on geometric arguments. Specifically, if the microtopographic elevation field on an ice-wedge polygon (IWP) is $Z_*(x, y)$, the the volumetric depth is

$$\Phi(\delta) = \frac{1}{A} \iint (\delta + Z_0 - Z_*(x, y)) H(\delta + Z_0 - Z_*(x, y)) dx dy \quad (1)$$

Where the integration is over the surface of the IWP, A is the area of the IWP, Z_0 is the minimum elevation in the IWP, and H is the Heaviside function. This could be computed from the microtopography and stored as a lookup table. Or, we could employ a simpler parameterization. To that end, we consider parameterizing the microtopography with two parameters:

(1) the elevation range spanned by the subgrid microtopography δ_{\max} , and

(2) the specific excluded volume δ_{ex} , which is the soil volume per unit bulk area. Then, we approximate the volumetric depth as

$$\Phi(\delta) = \begin{cases} (2\delta_{\max} - 3\delta_{\text{ex}}) \left(\frac{\delta}{\delta_{\max}}\right)^2 + (2\delta_{\text{ex}} - \delta_{\max}) \left(\frac{\delta}{\delta_{\max}}\right)^3 & \text{if } 0 \leq \delta \leq \delta_{\max}, \\ \delta - \delta_{\text{ex}} & \text{if } \delta > \delta_{\max}. \end{cases} \quad (2)$$

The IWP shown in Fig 1 was used to evaluate the parameterization Equation 2. The volumetric depth calculated from the approximation Equation 2 is compared (curve) with the direct calculation Equation 1 (dots) for an ice-wedge polygon in Figure 3. Also, shown is the volumetric depth in the

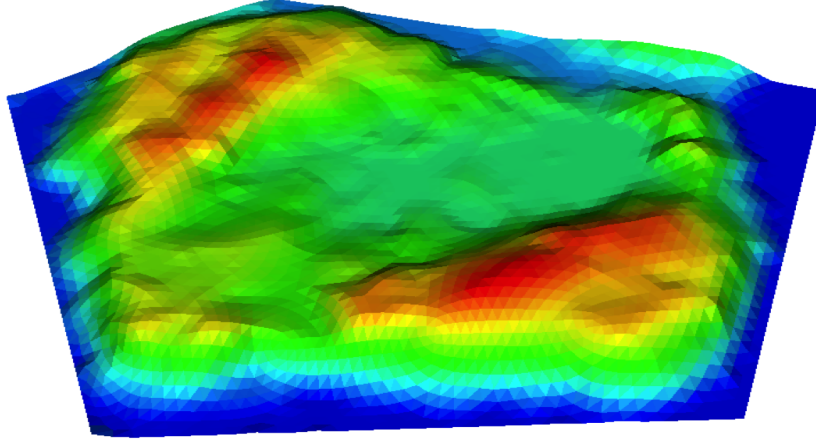


Figure 1: Microtopography for an example ice-wedge polygon from the Barrow Environmental Observatory (BEO).

absence of microtopography, which is linear with slope unity. Equation 1 is a very good approximation. Microtopographic effects on the flow law are not as straightforward to incorporate as the volumetric head $\Phi(\delta)$. In particular, we should make the distinction between depressions and obstructions (Panday and Huyakorn, 2004). Depressions are disconnected low points in the topography. The ponded depth must rise above the level of those depressions before any flow can happen. Obstructions exist above the depressions and interrupt and slow the flow, but do not block it completely. To model the effects of obstructions and depressions, we propose the following modification to the flow law

$$U = -\Theta(\delta) \frac{(\delta - \delta_d)^{2/3}}{n_{\text{mann}}(\|\nabla Z\| + \epsilon)^{1/2}} \quad (3)$$

where δ_d is the depression depth, and $\Theta(\delta) \in [0, 1]$ is a fractional conductance which account for flow reduction by obstructions. polygons-finescale

60 To calculate δ_d from the microtopography, we now propose an approach based on site percolation. Specifically, we fill the lowest elevation surface

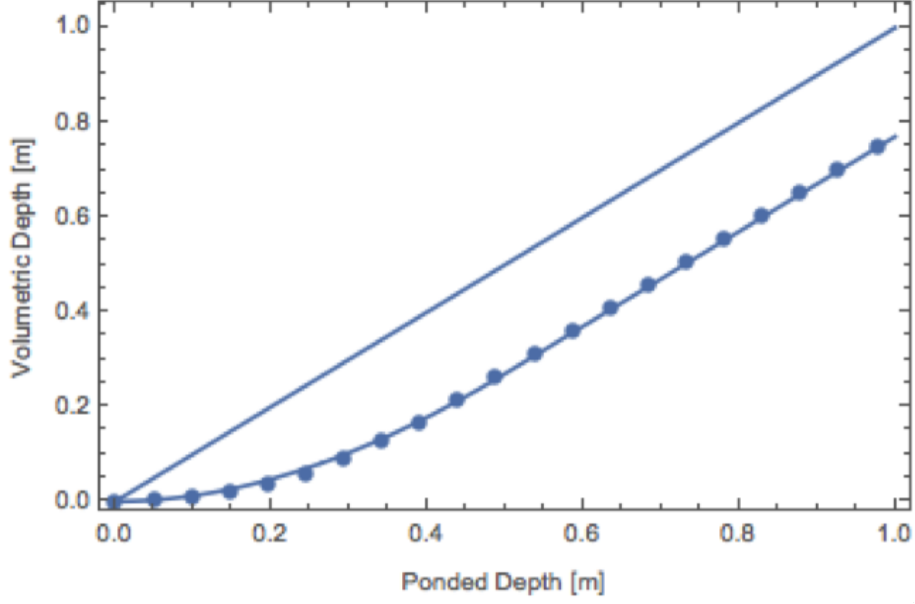


Figure 2: Volumetric depth versus ponded depth for polygon shown in Figure 1.

cells until the cluster of inundated cells spans the IWP. This is the percolation threshold. The water height at the percolation threshold defines the δ_d . Figure 4 shows the spanning cluster at the percolation threshold for the
65 IWP of Figure 1. The depression depth calculated this way is 4.1 cm for this IWP. It is reasonable to assume that the fractional conductance is well approximated by the fractional cross section available to flow, which can be estimated as the ratio of volumetric depth to ponded depth.

$$\Theta(\delta_d) \approx \frac{(\Phi(\delta) - \Phi(\delta_d))}{\delta} H(\delta - \delta_d) \quad (4)$$

Where H is the Heaviside function. The numerator is the flowing cross
70 sectional area. Note the velocity is multiplied by ponded depth to get a

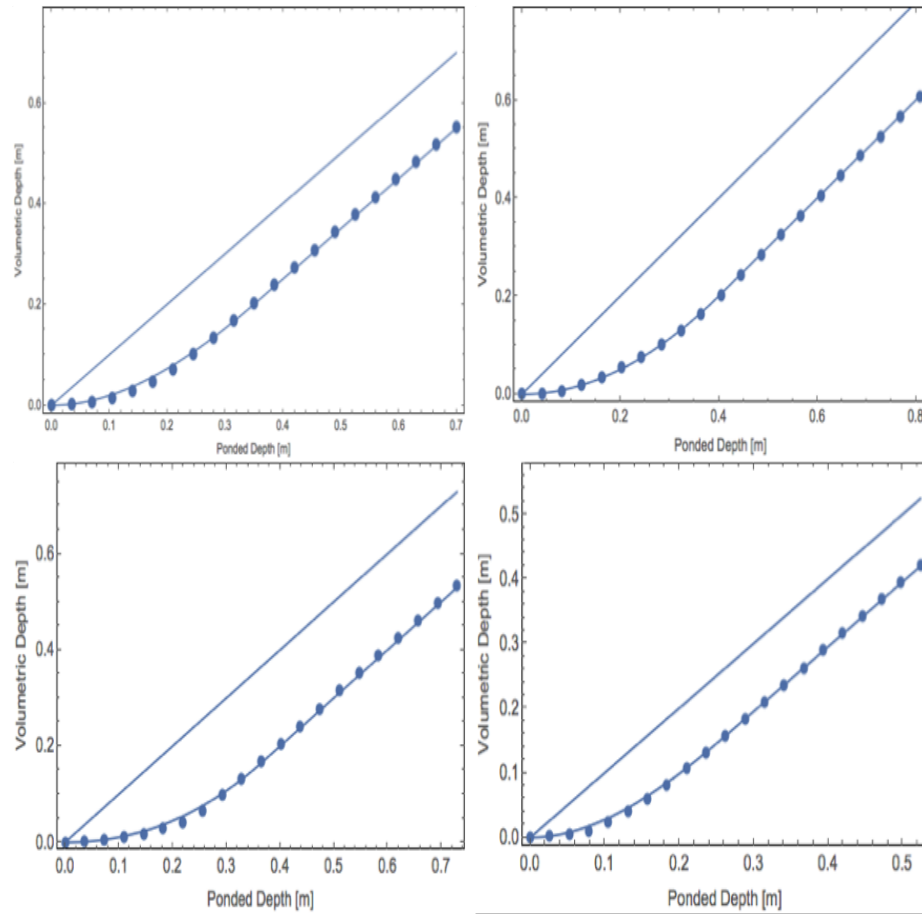


Figure 3: Volumetric depth versus poned depth for four additional ice-wedge polygons.

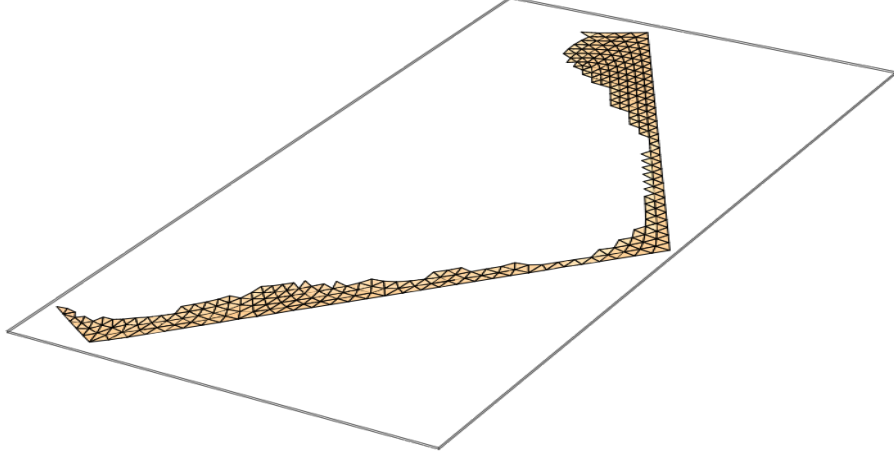


Figure 4: The spanning cluster at the percolation threshold for the IWP of Figure 1. The water depth relative to the low point of the microtopography at the percolation threshold defines the depression depth.

flux, so the molar flux appearing in the conservation equations becomes

$$\eta_l \delta U = -\eta_l (\Phi(\delta) - \Phi(\delta_d)) H(\delta - \delta_d) \Theta(\delta) \frac{(\delta - \delta_d)^{2/3}}{n_{\text{mann}} (\|\nabla Z\| + \epsilon)^{1/2}} \nabla(Z + \delta) \quad (5)$$

In summary, we hypothesize that the microtopographic effects on surface flow can be captured with a simple approximation with three parameters
75 that can be computed from the microtopography:

- Subgrid relief $\delta_{\text{max}} = Z_{*,\text{max}} - Z_{*,\text{min}}$, where $Z_{*,\text{max}}$ and $Z_{*,\text{min}}$ are the maximum and minimum elevation in the microtopography.
- Specific excluded volume δ_{ex} , the soil volume above the microtopographic low point normalized by IWP area.
- 80 • Depression depth δ , the difference between the maximum and minimum elevation of the cells in the spanning cluster at the percolation

threshold.

The subgrid relief and specific excluded volume come directly from the microtopography (univariate statistics). The depression depth requires a simple percolation algorithm to identify the spanning cluster at the percolation threshold. Values are given in Table 1.

Table 1: Parameters used in the subgrid model

	C06	C31	C40	C44	C45	A0	B01
$\delta_{\max}(m)$	0.404	0.262	0.483	0.364	0.350	0.361	0.411
$\delta_{\text{ex}}(m)$	0.2	0.105	0.23	0.2	0.15	0.185	0.26
$\delta_{\text{d}}(m)$	0.069	0.128	0.043	0.187	0.164	0.222	0.143

3. The Advanced Terrestrial Simulator (ATS)

Here we provide a very brief overview of the ATS for a reference, for more details about the software infrastructure we refer the reader to [6, 7]. A fully integrated surface/subsurface and snow distribution modeling capability implemented in ATS are available here [3, 8]. In addition, a mixed-dimensional modeling strategy, mainly designed for the simulations of low-relief permafrost-affected regions, can be found here [9]. The ATS is a publically-available massively parallel computer code, an extended version of Amanzi (flow and reactive transport simulator; see [10]), based on process management tool called Arcos. In ATS, a process kernel (PK) refers to governing mathematical equations representing a particular (or coupled)

physical process(es). Further, Multiprocess Coordinators (MPCs) are avail-
100 able to facilitate coupling among PKs. This framework allows to dynam-
ically build a complex/coupled hierarchical model structure. The flexible
extensibility feature of the Arcos framework allowed to easily implement
our subgrid model and couple with the existing PKs.

4. Numerical Results and Discussions

105 4.1. Simulations

To assess the accuracy of the numerical results of our subgrid model, we
compare our results with fine-scale simulations. . the results of seven fine-
scale ice-wedge polygons and no subgrid results. To point out, the entire
fine-scale IWP is considered as one grid cell in the subgrid and no subgrid
110 model – the slope depends on the elevation of the corners of the fine-scale
IWP. For demonstration purpose, we consider surface-only flow simulations.
In our work, the seven ice-wedge polygon for fine-scale simulations are con-
sidered from Barrow Environmental Observatory (BEO) and illustrated in
Figures 2 and 5. These polygons consist of low-center, high-center, with
115 well established troughs (relatively uniform elevation across the trough) and
obstructions in the troughs, and hence represent a broader class of polyg-
onal landscape. Three sets of numerical results of the subgrid model are
presented:

We also show that the subgrid model results are more closer than the no
120 subgrid model the no subgrid simulations underestimates the water content.

Study I: Subgrid uncalibrated results;

Study II: Subgrid results with calibrated values of the depression depth
listed in Table 1;

Study III: Subgrid simulations with calibrated values of the depression
125 depth and the manning coefficient.

Study II is motivated by fine-scale simulations, higher depression depth
may delay breakthrough, and would lead to more accumulation of water in
the depressions. That said, in Study II we adjust the value the depression
depth computed by the percolation algorithm to provide a better fit to the
130 fine-scale results. The process of adjusting model’s parameters to replicate
the benchmark (e.g., fine-scale computational or real experiments) results
is known as calibration. Moreover, higher pressure in the subgrid model
affects the overland conductivity and hence the discharge rate. To mimic
the behavior of the fine-scale at the time of breakthrough and the recession
135 period, the surface roughness is decreased by raising the manning coefficient
in the governing equation. This analysis proposed Study III.

Numerical simulations are performed for a “pulse numerical test” sce-
nario – injection followed by recession. In other words, we start with a
fully dry surface, and inject water at a constant rate at the inlet boundary
140 until breakthrough happens (prescribed flux boundary for a certain period
of time), then stop the water supply and let water pass through the outlet
(free drainage boundary). The arrows shown in Figure 5 indicate the inlet
and outlet boundaries. The rainfall events are not considered. The presence
of depression depth parameter in the flow law of our subgrid model will
145 not allow to replicate the shape of the hydrograph because the fine-scale
simulations will show immediate breakthrough. To capture such a behavior
it would be more practical to determine the value of the depression depth
dynamically – change the depression depth as the ponded depth changes.

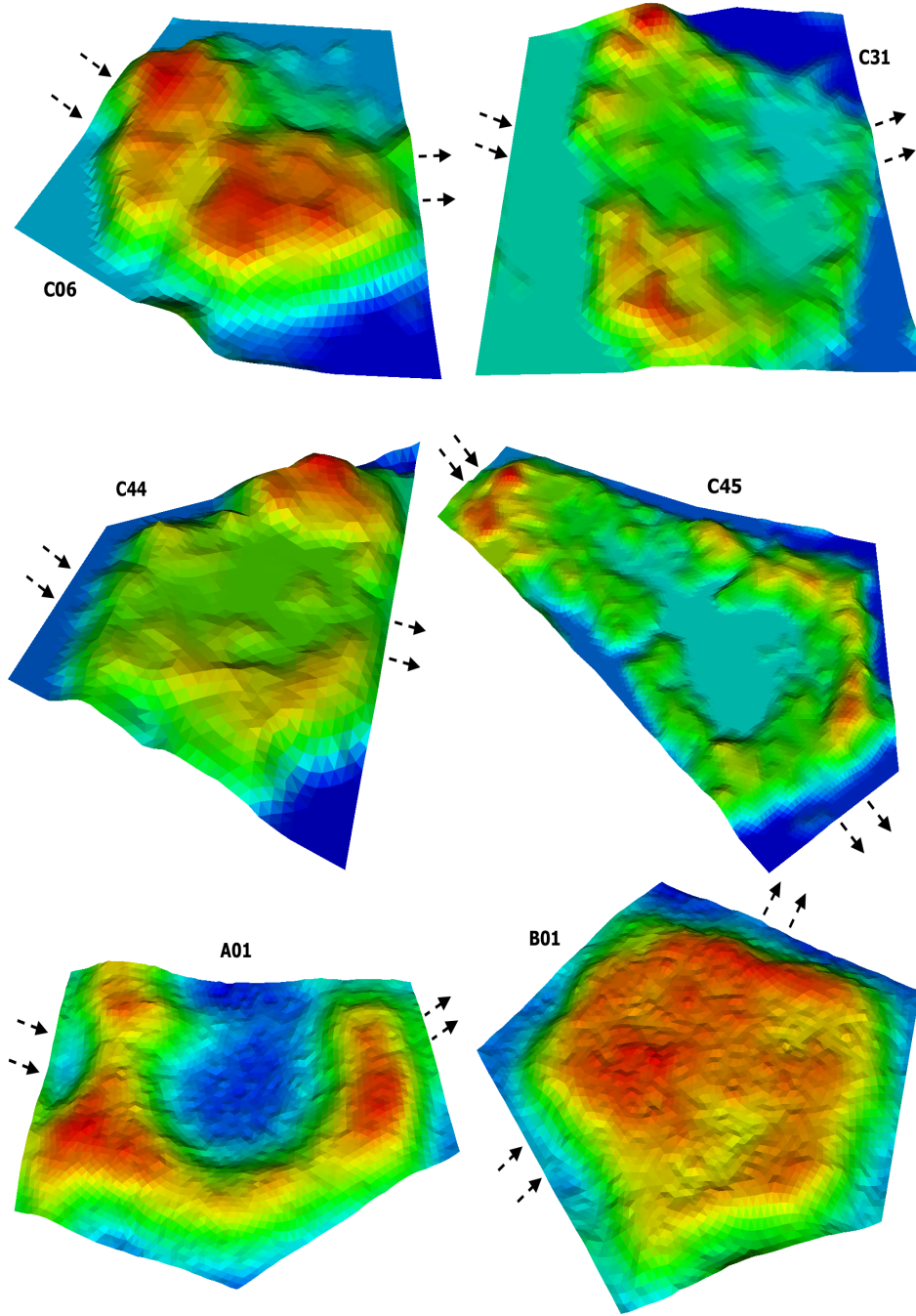


Figure 5: An Illustration of the microtopography for ice-wedge polygons from Barrow Environmental Observatory (BEO). Red and dark blue spots correspond to high- and low-elevated regions. The arrows indicate inlet and outlet boundaries.

4.2. Results and Discussions

150 Numerical results presented here correspond to the three studies mentioned above. We compare our results with fine-scale simulations of single IWPs, and we do not present any results on a cluster of fine-scale IWPs. We have carried out detailed simulations on all the polygons shown in Figure 5, however, we discuss the results of polygon C44 in more detail and these
155 results serve as a representative of all the remaining polygons as far as the accuracy and shape of the hydrographs are concerned. Figure 6 compares the numerical results of the subgrid model with the fine-scale simulations, and no subgrid model of polygon C44. Clearly, Study I fails to match the fine-scale simulations, delayed breakthrough in the subgrid model is an indication of higher depression depth computed by the percolation algorithm;
160 see Figure 6(a). Simulations with a calibrated depression depth, Study II, dramatically improve the shape of the hydrograph and the water content in the system as highlighted in see Figure 6(b). However, a mismatch appears at the time of breakthrough and the beginning of the recession period even
165 with the calibrated depression depth. As alluded to earlier, this is due to the huge head gradient between the center and the seepage face, and physically makes sense. Figure 6(c) illustrates the results of Study III, and it is evident that our subgrid model reproduces the fine-scale behavior, and the numerical results are identical.

170 Figure 7 compares the numerical results of Study I and III with the fine-scale and no subgrid model. The percolation algorithm computed the depression depth very accurately for polygon C06, and calibration (Study II) is not required. Similar to the results of polygon C44, the high over-land conductivity in the subgrid model is reduced by increasing the surface
175 roughness. It improves the results and replicate the recession period of the

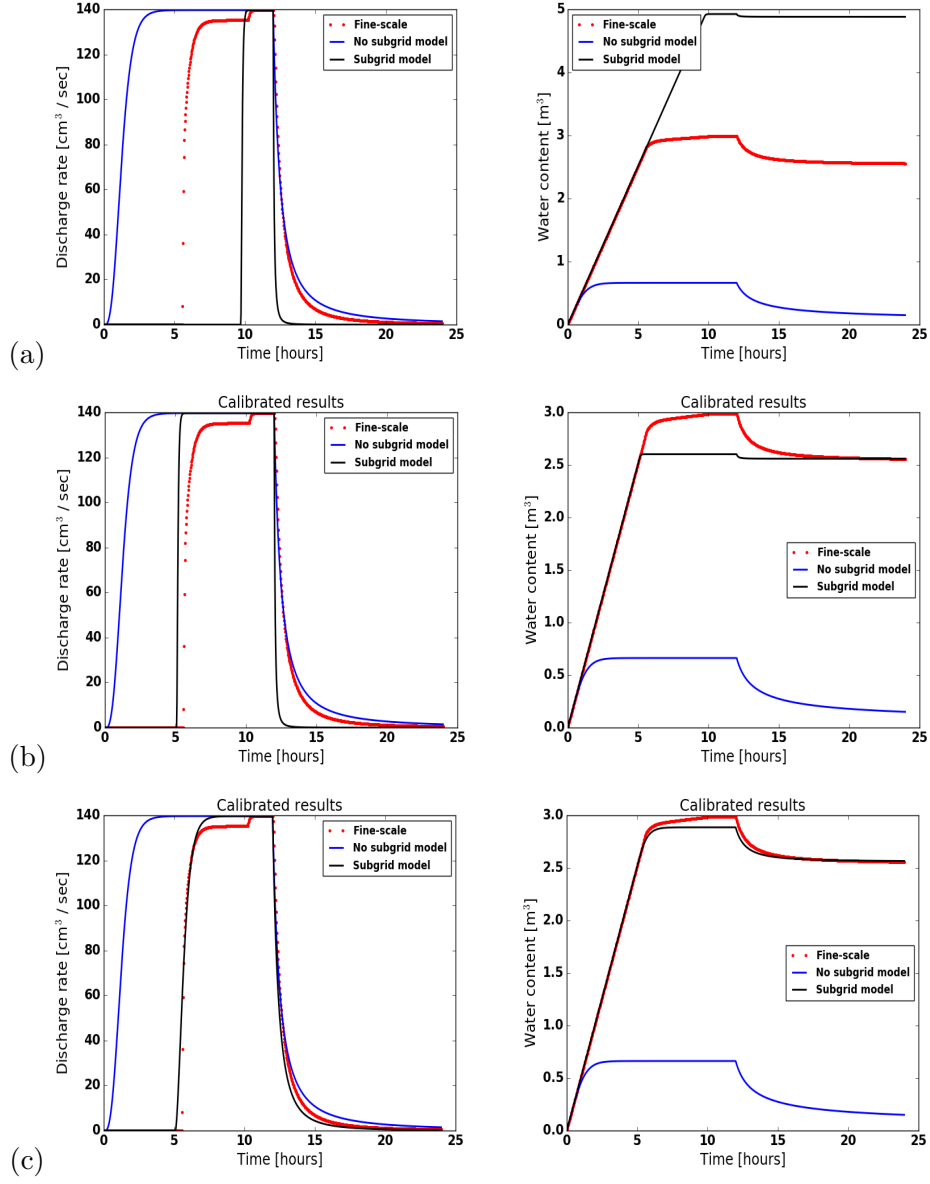


Figure 6: (Polygon C44) Comparison of the numerical results of the subgrid model with the fine-scale and without subgrid model results. Rows (top to bottom) correspond to Study I, II and III, respectively.

fine-scale results. It is important to see the amount of water (not available for drainage) in the system after the recession period. Figure 7 also displays the water retained the in subgrid model and the fine-scale model – the match is very close. For polygon C31, the results of the subgrid model are strongly
180 affected by the depression depth in Study I, and lead to a mismatch. However, the results of Study II and III indicate that calibrated values of the depression depth and the surface roughness improved the simulated results dramatically and yield a close match as depicted in Figure 8. Numerical simulations correspond to polygons C31, C45, A01, and B01 are shown in
185 Figures 8, 10, 11(a), and 12, respectively. Overall, the results of the subgrid model are very encouraging and consistently yield a better fit to the fine-scale results as compared to the no subgrid model.

4.3. Additional Remarks

- Not surprisingly, the subgrid model favors high surface roughness that
190 swings the results toward fine-scale simulations. A high agreement between the results of the subgrid model and fine-scale simulations due to reduced runoff is an indication of a needed drag coefficient in the flow law. A linear regression fit to the calibrated manning coefficient vs. the depression depth is depicted in Figure 13. The fit indicates
195 higher depressions require larger drag coefficient.
- For low-centered polygons such as C45 and A01, Study I (uncalibrated results) fails to match the hydrograph of the fine-scale simulations – no breakthrough happens for the uncalibrated depression depths. Fine-scale simulations show that low-elevated regions may remain com-
200 pletely dry if they are not located in the main flow channel which trivial. However, as stated earlier, our percolation algorithm fills the

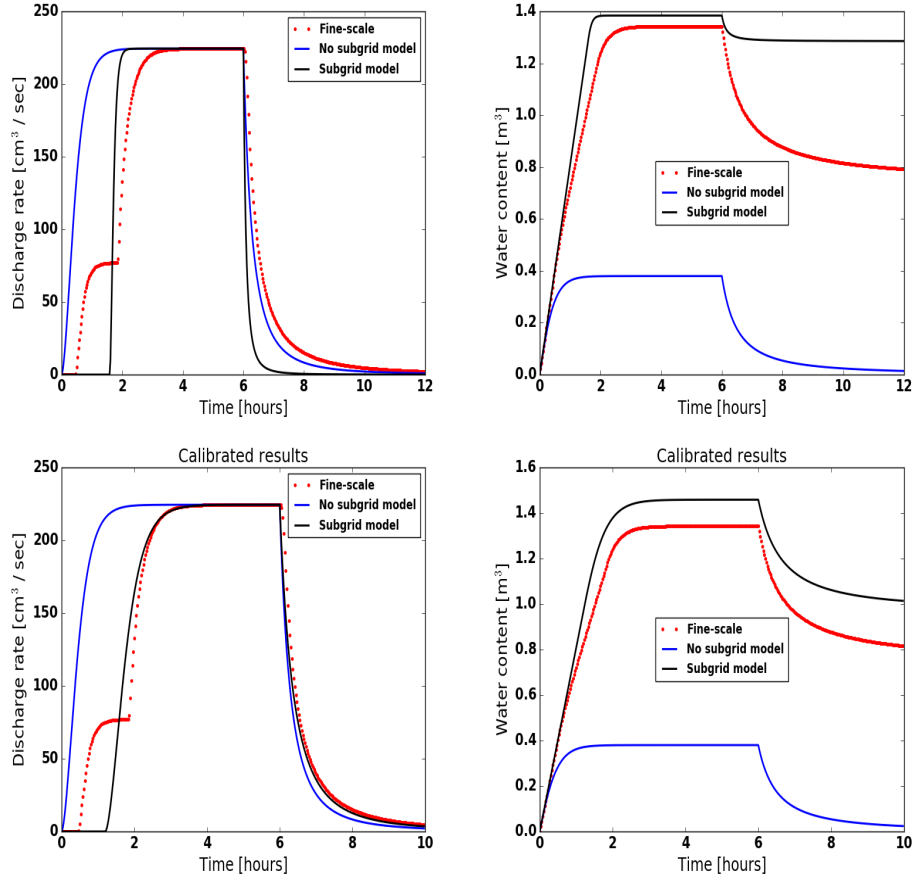


Figure 7: (Polygon C06) Comparison of the numerical results of the subgrid model with the fine-scale and without subgrid model results. Top and bottom row correspond to Study I and Study III, respectively.

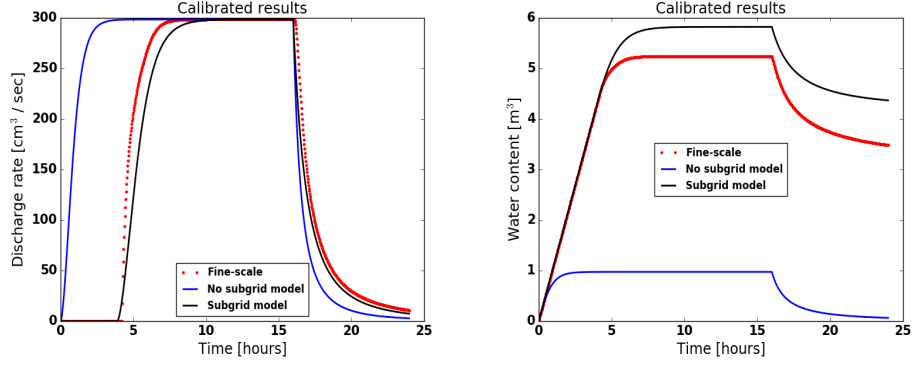


Figure 8: (Polygon C31) Comparison of the numerical results of the subgrid model with the fine-scale and no subgrid model. Results corresponded to Study III.

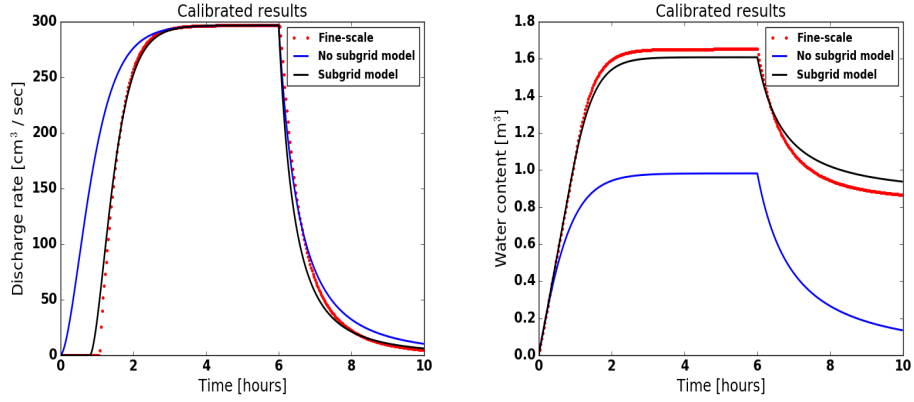


Figure 9: (Polygon C40) Comparison of the numerical results of the subgrid model with the fine-scale and without subgrid model results. Bottom row displays calibrated results.

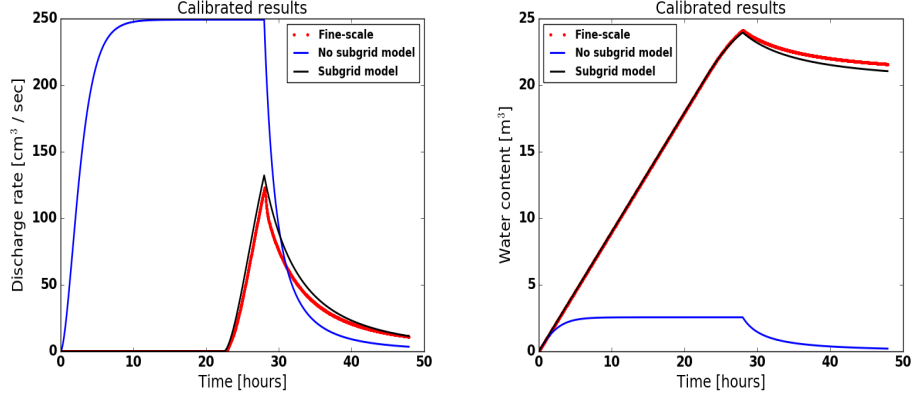


Figure 10: (Polygon C45) An illustration of the numerical results of the subgrid model, the fine-scale and no subgrid model. The simulations correspond to Study III.

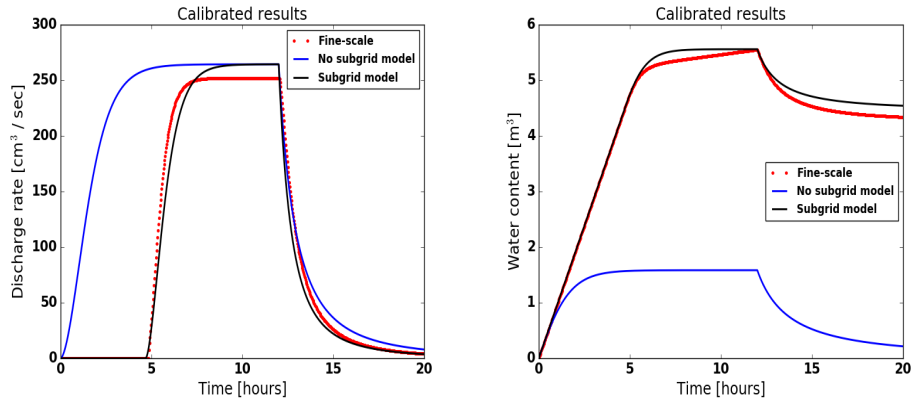


Figure 11: (Polygon A01) Comparison of the hydrographs and water content from the numerical simulation of the fine-scale, subgrid and no subgrid models.

lowest elevation cells until the cluster of inundated cells spans the IWP. Thereby, the direction of the injected fluid is important. For instance, considering polygon A01, the results are not comparable if the inlet and outlet are at sides inlet_1 and outlet_1 , respectively. However, if the inlet and outlet are switched to inlet_2 and outlet_2 a desirable match is

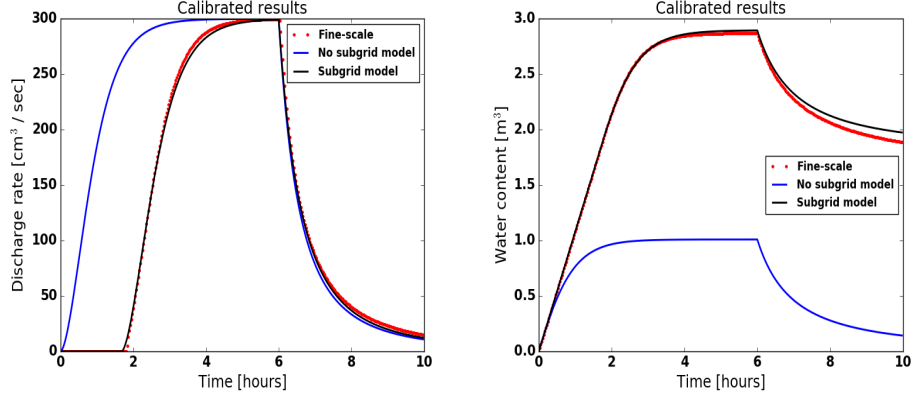


Figure 12: (Polygon B01) Comparison of the numerical results of the subgrid model with the fine-scale and without subgrid model results.

obtained; see Figure 14.

- Application of invaded percolation (flow in the direction of least resistance) algorithm could provide more accurate depression depths, and would probably overcome the issue of calibrating parameters and/or location of inlet and outlet boundaries.
- Most of our numerical experiments show that the subgrid model always performs better than the no subgrid model even if they are not reasonably closed to the fine-scale simulations.
- When the inlet boundary has obstructions (for example, polygon C06 in Figure 5) and divides the incoming water into different flow channels, the water reaches the outlet boundary at different times and lead to a dual-peak (or may be multiple peaks) hydrograph. Due to only one grid cell in the subgrid model, the dual-peak behavior is not possible to capture.

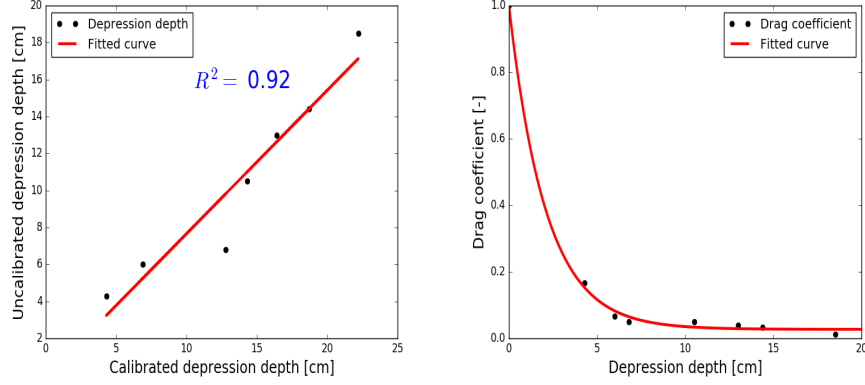


Figure 13: (Left) Linear fitted-curve to the depression depth data.

5. Conclusions

The subgrid model presented in this paper is aimed at incorporating the microtopographic effects in the governing equations for the simulations at watershed scale. The comparative analysis of the subgrid results with the fine-scale IWP results reveal that our model has the potential to accurately represent fine-scale flow behavior at larger spatial scales.

References

- [1] S. Painter, J. Moulton, C. Wilson, Modeling challenges for predicting hydrologic response to degrading permafrost, *Hydrogeology Journal* (2013) 1–4.
- [2] B. L. Kurylyk, K. T. MacQuarrie, J. M. McKenzie, Climate change impacts on groundwater and soil temperatures in cold and temperate regions: Implications, mathematical theory, and

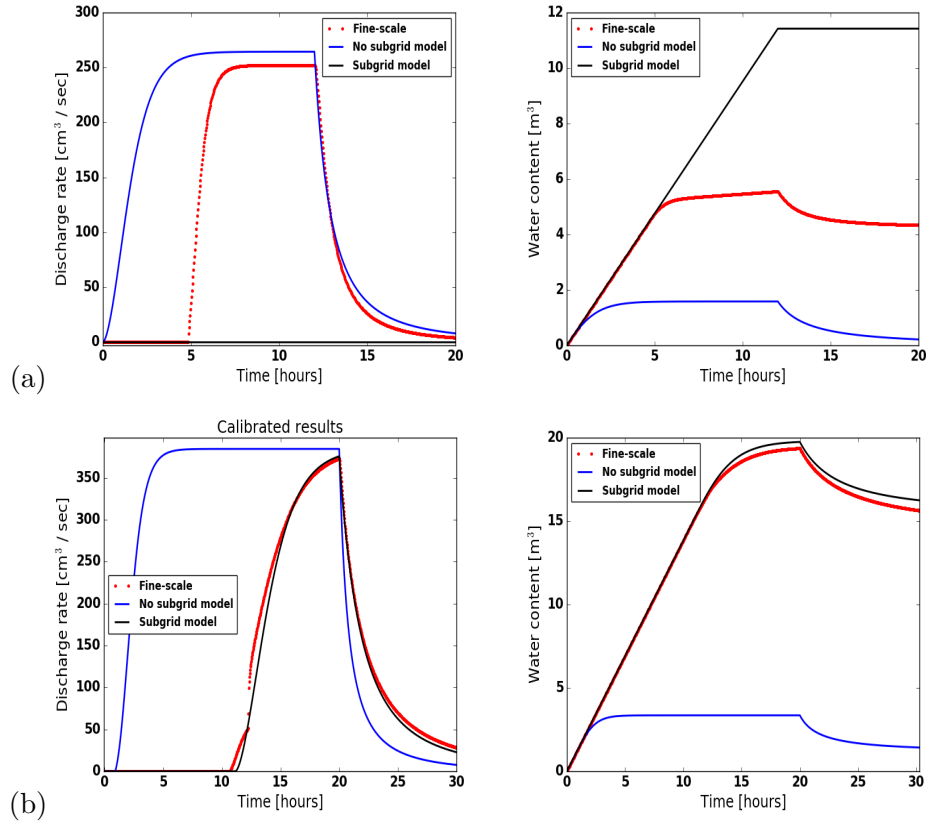


Figure 14: (Polygon A01) An illustration of the choice of the inlet and outlet boundaries on the numerical results. The orientation affects the match between the fine-scale and subgrid model. (a) inlet₁ and outlet₁ boundary; (b) inlet₂ and outlet₂ boundary.

235

emerging simulation tools, *Earth-Science Reviews* 138 (2014) 313–334.

- [3] S. L. Painter, E. T. Coon, A. L. Atchley, M. Berndt, R. Garimella, J. D. Moulton, D. Svyatskiy, C. J. Wilson, Integrated surface/subsurface permafrost thermal hydrology: Model formulation and proof-of-concept simulations, *Water Resources Research* 52 (2016) 6062–6077.

240

- [4] W. N. Stammers, H. Ayers, The effect of slope and microtopography on depression storage and surface detention, publisher not identified, 1956.
- 245 [5] S. Panday, P. S. Huyakorn, A fully coupled physically-based spatially-distributed model for evaluating surface/subsurface flow, *Advances in water Resources* 27 (2004) 361–382.
- [6] E. T. Coon, J. D. Moulton, S. L. Painter, Managing complexity in simulations of land surface and near-surface processes, *Water*
250 *Resources Research* 78 (2016) 134–149.
- [7] E. T. Coon, *ATS: The Advanced Terrestrial Simulator*, 2016.
<http://github.com/amanzi/ats>.
- [8] A. L. Atchley, S. L. Painter, D. R. Harp, E. T. Coon, C. J. Wilson,
255 A. K. Liljedahl, V. E. Romanovsky, Using field observations to inform thermal hydrology models of permafrost dynamics with ats (v0.83), *Geoscientific Model Development* 8 (2015) 2701–2722.
- [9] A. Jan, E. T. Coon, P. S. L., R. Garimella, J. D. Moulton,
260 An intermediate-scale model for thermal hydrology in low-relief permafrost-affected landscapes, Submitted to *Computational Geosciences* (2016).
- [10] J. D. Moulton, M. Berndt, R. Garimella, L. Prichett-Sheats,
G. Hammond, M. Day, J. Meza, High-level design of amanzi, the multi-process high performance computing simulator, office of environmental management, united states department of energy, washington dc (2012).
265